Clinical Radiology 86 (2025) 106934

Contents lists available at ScienceDirect

Clinical Radiology

journal homepage: www.clinicalradiologyonline.net

Differential diagnosis between parotid pleomorphic adenoma and basal cell adenoma based on CT-enhanced histogram analysis

L. Han, M. Ma, H. Liu, Q. Zhang, Y. Zhang, X. Liu, X. Wu*

Department of Radiology, Xi'an Central Hospital Affiliated to Xi'an Jiaotong University, Xi'an 710003, Shaanxi, China

ARTICLE INFORMATION

Article history:
Received 10 September 2024
Received in revised form
18 March 2025
Accepted 14 April 2025

AIM: To explore the application value of differentiating pleomorphic adenoma (PA) of parotid gland from basal cell adenoma (BCA) based on computed tomography (CT)-enhanced histogram parameters.

MATERIALS AND METHODS: This retrospective study included 55 patients with PA and 35 patients with BCA confirmed by surgery and pathology. All patients underwent noncontrast CT and dual phase CT-enhanced scan. FireVoxel software was used to delineate the tumour parenchyma and perform histogram analysis, obtaining nine histogram parameters: mean, variance, skewness, kurtosis, and the 1st, 10th, 50th, 90th, and 99th percentiles. To compare the differences of histogram parameters between PA and BCA groups in parotid gland, and draw receiver operating characteristic (ROC) curve to analyse the diagnostic efficiency of histogram parameters in differentiating PA from BCA.

RESULTS: The 1st percentile of noncontrast, mean of arterial phase, variance of arterial phase, 10th, 50th, 90th and 99th percentile of arterial phase and mean of venous phase were significantly higher in the BCA group compared with the PA group ($P<0.05$). ROC curve analysis showed that arterial phase histogram parameters exhibited better diagnostic efficiency in distinguishing PA from BCA when compared with noncontrast, arterial phase and venous phase. Among them, the 90th percentile of arterial phase has the best differential diagnosis efficiency. When the cutoff value is 132.00×10^{-6} mm^2/s, the area under the curve is 0.876, the sensitivity and specificity of distinguishing PA from BCA are 90.50% and 84.00%, respectively.

CONCLUSION: CT-enhanced histogram analysis demonstrates diagnostic value in differentiating PA from BCA and may contribute to optimised clinical decision-making.

* Guarantor and correspondent: X. Wu, Medical Imaging Center of Xi'an Central Hospital affiliated with Xi'an Jiaotong University, No.161, Xiwu Road, Xincheng District, Xi'an 710003, China.
E-mail address: szping518@163.com (X. Wu).

https://doi.org/10.1016/j.crad.2025.106934

Introduction

Pleomorphic adenoma (PA), also known as a mixed tumour, is the most common benign tumour of the salivary glands, accounting for about 50%–70% of salivary gland tumours.[1,2] Histologically, it is composed of glandular epithelial and myoepithelial cells mixed with mucoid or mucochondroid stroma, characterised by the diversity of cell morphology and structure.[3] Basal cell adenoma (BCA) ranks third among benign tumours of the salivary glands. Unlike PA, BCA is primarily composed of basal-like cells, lacking a mucochondroid matrix.[4] Based on the cell growth pattern, BCA is divided into four pathological subtypes: solid, tubular, trabecular and membranous. These subtypes demonstrate the diversity within the tumour.[5] Currently, computed tomography (CT) and magnetic resonance imaging (MRI) examination techniques have made significant progress in distinguishing PA and BCA, as well as accurately reflecting the relationship between tumours and surrounding tissues.[6,7,8] However, there are many morphological overlaps between PA and BCA, which affect the objectivity of differential diagnosis results. Given the high malignant transformation and recurrence rates of PA, radical resection is preferred in clinical practice. In contrast, the prognosis of BCA is better, and the risk of postoperative recurrence is lower.[9,10,11] Therefore, it is crucial to make a definitive diagnosis of PA and BCA before surgery to ensure effective clinical treatment.

Differences in pathological tissue and cell structures among various tumours lead to distinct heterogeneity. Radiomics histogram analysis can effectively evaluate tumour heterogeneity by quantitatively analysing the spatial relationships and grey-level distributions of pixels in extracted images.[12,13] Currently, some researchers have identified PA and BCA using MRI deep learning models,[14] but few studies have explored their identification based on CT-enhanced histogram analysis. Compared with MRI, CT offers distinct advantages in radiomics analysis of parotid masses, including faster image acquisition, wider clinical applicability (e.g. tolerance in patients with MRI contraindications) and the opportunity to retrospectively analyse incidental parotid lesions identified in CT scans performed for unrelated clinical purposes. Therefore, this study aims to analyse the radiomics histogram parameters of CT-enhanced images to explore their application value in distinguishing PA from BCA.

Materials and methods

Study subjects

This retrospective study included 55 patients with PA and 35 patients with BCA; all confirmed by surgery and pathology at our institution. Inclusion criteria is as follows: (1) All patients underwent noncontrast CT scan and dual-phase enhanced CT scan before the operation. (2) All patients had newly diagnosed PA and BCA confirmed by pathology. (3) Complete clinical and imaging data were available. Exclusion criteria is as follows: (1) Patients who had received puncture, radiotherapy, or chemotherapy before the CT examination. (2) Images with significant artifacts. (3) Incomplete pathological sections.

This retrospective study was approved by our institutional review board and informed consent was waived.

CT-scanning protocol

CT images were acquired on a 256-row CT scanner (Philips Brilliance iCT 256; Philips Healthcare, Best, The Netherlands). The scanning range is from the external ear hole to the lower edge of mandible. The scanning parameters were as follows: tube voltage, 120 kV; tube current, 250–300 mA; reconstruction layer thickness, 1mm; reconstruction matrix, 512 × 512. During enhancement scanning, all patients received intravenous injection of contrast agent (Iohexol; 300mgI/kg; GE Healthcare; 1.5–2.0 mL/kg, with an injection rate of 2.5 mL/s). Then, 25 mL normal saline was injected with the same injection rate. The delay times for the arterial and venous phases were fixed at 30–35 and 55–60 seconds after the contrast agent injection, respectively.

Image analysis

Images were analysed on the post-processing workstation (Extended Brilliance Workspace [EBW]; Philips Healthcare, Best, The Netherlands). Conventional CT characteristics were assessed and analysed on the images of noncontrast (NC). The morphologic characteristics were as follows: maximum diameter, lesion shape, density, location, boundary and calcification. CT values of tumour parenchyma in different periods were measured. Then calculate the arterial phase CT enhancement value and venous phase CT enhancement value. According to the Δ CT formula: Δ CT AP=CT AP-CT NC; Δ CT VP=CT VP-C T NC.

Tumour histogram analysis was performed using the FireVoxel software (https://firevoxel.org/download/). Two experienced head and neck radiologists analysed and manually draw the region of interest (ROI) without knowing the pathological results. To better evaluate tumour heterogeneity,[15] ROI should encompass all tumour information, including necrosis, calcification and haemorrhage. Additionally, the ROI outlined area should be slightly smaller than the visible tumour boundary, considering the effect of partial volume effects. Subsequently, the largest lesion slice was selected. ROIs were drawn along the edges of the tumour on axial CT images, and filling the contours with red.[16] Histogram data were automatically generated by using FireVoxel software for each ROI and these parameters include the following: mean, variance, skewness, kurtosis, and the 1st, 10th, 50th, 90th and 99th percentiles. Typical cases of PA and BCA are shown in Figs 1 and 2, respectively. The corresponding histograms for PA and BCA are shown in Supplementary Figs 1 and 2.

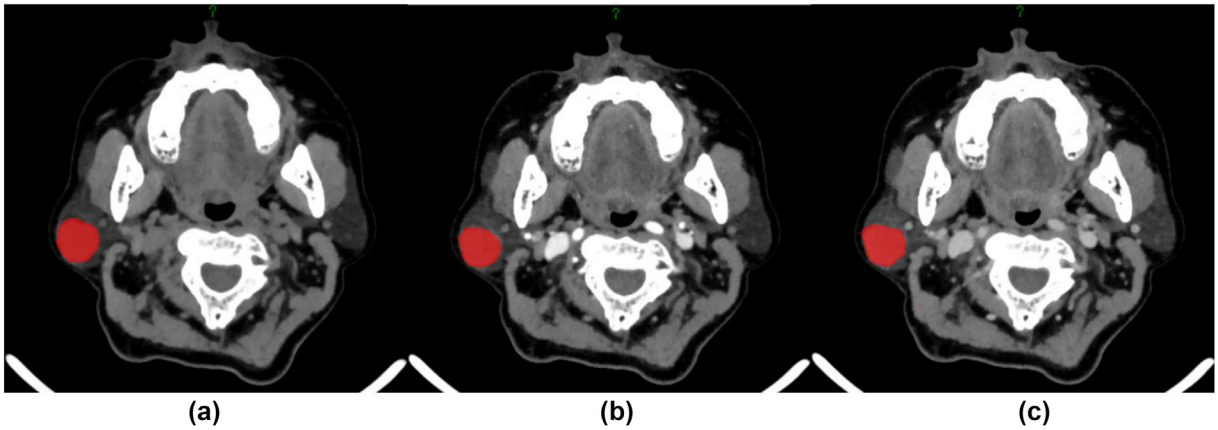

Figure 1 A 45-year-old female patient with a right parotid pleomorphic adenoma. In (a), the ROI is delineated on the noncontrast CT image. Similarly, in (b) and (c), the ROI is delineated on the arterial phase and venous phase CT images, respectively. CT, computed tomography; ROI, region of interest.

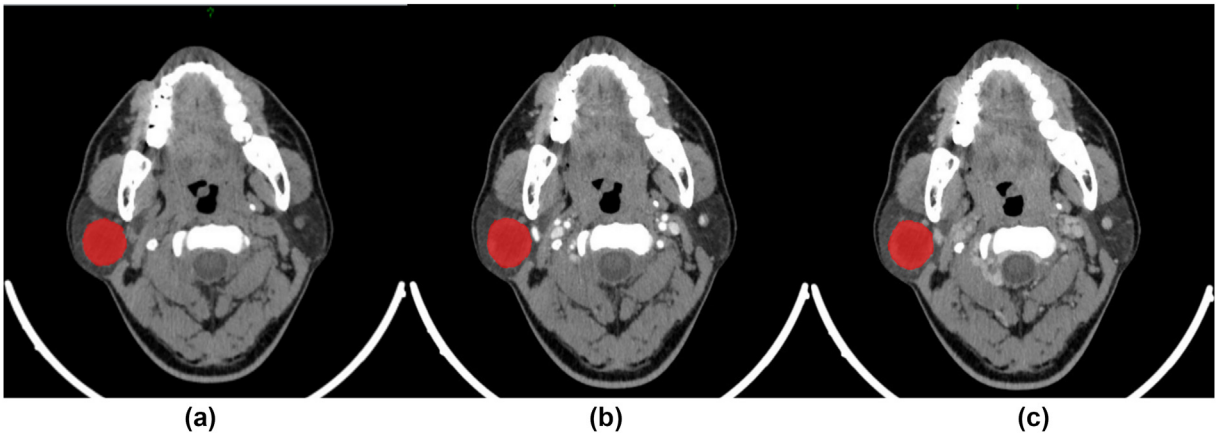

Figure 2 A 53-year-old female patient with a right parotid basal cell adenoma. In (a), the ROI is delineated on the noncontrast CT image. Similarly, in (b) and (c), the ROI is delineated on the arterial phase and venous phase CT images, respectively. CT, computed tomography; ROI, region of interest.

Pathological diagnosis

The pathological diagnosis was established through histopathological examination of surgical specimens. All specimens were independently reviewed by two experienced pathologists with more than 10 years of expertise in salivary gland pathology, according to the World Health Organization (WHO) classification of head and neck tumours (5th edition, 2022).[17] PA was characterised by a mixed proliferation of epithelial and mesenchymal components, including glandular structures, myxoid and chondroid matrix. BCA was diagnosed based on the presence of basaloid cells arranged in solid, trabecular, tubular, or membranous patterns and the absence of myxoid or chondroid stroma. Any discrepancies in diagnosis were resolved through consensus discussion.

Statistical analysis

SPSS 23.0 software was used for statistical analyses. The Shapiro–Wilk test was employed to assess normality of histogram parameters. Parameters with normal distribution were expressed as $\overline{x} \pm s$ and compared using the independent sample *t* test. Nonnormal parameters were expressed as median (Q1, Q3) and compared using the Mann–Whitney U test. The χ^2 test was used to analyse differences in categorical data. The inter-observer reliability of histogram parameters was assessed using the intra-class correlation coefficient (ICC), with an ICC index > 0.75 indicating high consistency. Receiver operating characteristic (ROC) curves were constructed to assess the diagnostic performance of histogram parameters, providing area under the curve (AUC), sensitivity and specificity. The

diagnostic efficiency in differentiating between PA and BCA preoperatively was evaluated. A *P* value of less than 0.05 was considered statistical significance. To determine whether the efficiency differences between the combined AP model and the non-AP phases, the DeLong test was applied.

Results

General data comparison

PA patients' mean age was 41.50 ± 15.25 years, while BCA patients' mean age was 53.00 ± 9.38 years. This difference was statistically significant ($P<0.05$). No significant differences were found between PA and BCA in terms of tumour maximum diameter, location, calcification, single tumour, boundary, shape, density and noncontrast CT (NCCT) value ($P>0.05$). The differences between PA and BCA in CT AP, CT VP, ΔCT AP, and ΔCT VP were statistically significant ($P<0.05$). The clinical features and routine CT signs of PA and BCA patients are shown in Table 1.

Inter-observer agreement

The inter-observer agreements calculated by appropriate statistical methods. The mean, variance, skewness, kurtosis and all percentile values showed excellent inter-reader agreement (ICC: 0.812−0.905).

Table 1
Clinical data and conventional CT features of PA and BCA.

	PA	BCA	t/χ^2	*P*
Age	41.50 ± 15.25	53.00 ± 9.38	3.216	0.003
Maximum diameter	2.83 ± 0.36	2.32 ± 0.45	1.736	0.507
Location			0.011	0.915
Superficial	27	18		
Deep	28	17		
Number			0.043	0.836
Single	52	33		
Multiple	3	2		
Calcification			0.212	0.645
With	52	34		
Without	3	1		
Boundary			0.013	0.911
Clear	50	32		
Unclear	5	3		
Shape			0.029	0.865
Round	45	29		
Non-round	10	6		
Cystic areas			0.619	0.431
With	29 (52.7%)	23 (65.7%)		
Without	26 (47.3%)	12 (34.3%)		
NCCT	31.55 ± 10.25	36.45 ± 11.40	-1.570	0.123
CT AP	47.31 ± 13.99	82.95 ± 23.34	-6.661	<0.001
CT VP	64.82 ± 18.26	95.10 ± 25.24	-4.875	<0.001
ΔCT AP	15.93 ± 7.85	46.35 ± 22.10	-5.903	<0.001
ΔCT VP	33.55 ± 13.20	58.20 ± 25.98	-3.909	0.001

BCA, basal cell adenoma; CT, computed tomography; PA, pleomorphic adenoma.

Comparison of histogram parameters between PA and BCA

The 1st percentile of noncontrast BCA was significantly higher than that of PA, with a significant statistically difference ($P<0.05$). The mean, variance, 10th, 50th, 90th and 99th percentiles of BCA during the arterial phase were all higher than those of PA, with statistically significant differences ($P<0.05$). In the venous phase, the average value of BCA was higher than that of PA, with statistically significant differences ($P<0.05$). The comparison of histogram parameters between PA and BCA is shown in Table 2.

ROC curve analysis

The histogram parameters with statistical significance were analysed by an ROC curve, and their corresponding AUC, sensitivity and specificity are shown in Table 3 and Fig 3. The 1st percentile of NC, the mean, variance, 10th, 50th, 90th and 99th percentile of AP, as well as the mean of VP have high diagnostic efficiency in differentiating PA from BCA before operation. In the comparison of NC, AP and VP histogram parameters, the AP histogram parameters show better diagnostic efficiency. Among them, the 90th percentile of AP exhibits the best differential diagnosis efficiency. When the cutoff value is 132.00 × 10-6 mm^2/s, the AUC value

Table 2
Comparison of histogram parameters between PA and BCA.

Parameters	PA	BCA	*t/Z*	*P*
NC				
Mean	102.07 ± 9.77	105.45 ± 7.63	-1.300	0.200
Variance	134.26 ± 51.42	106.94 ± 55.47	1.574	0.125
Skewness	1.51 (-2.36,-0.85)	1.25 (-1.91,-0.66)	-1.542	0.123
Kurtosis	7.92 ± 14.44	3.52 ± 2.65	1.340	0.187
1st percentile	58.84 ± 17.31	70.25 ± 15.86	-2.302	0.026
10th percentile	86.36 ± 15.08	92.70 ± 11.47	-1.601	0.117
50th percentile	103.28 ± 11.16	106.7 ± 7.33	-1.234	0.224
90th percentile	113.0 ± 10.73	116.45 ± 6.37	-1.388	0.188
99th percentile	121.08 ± 11.28	134.9 ± 34.09	-1.738	0.096
AP				
Mean	113.36 ± 12.46	141.49 ± 23.36	-4.865	<0.001
Variance	196.53 ± 101.96	286.33 ± 75.51	-2.820	0.009
Skewness	1.49 (-1.72,-0.22)	0.96 (-1.25,-0.91)	-0.620	0.535
Kurtosis	3.76 (1.43,5.19)	3.79 (0.34,3.36)	-1.810	0.069
1st percentile	67.84 ± 22.40	80.60 ± 25.89	-1.755	0.087
10th percentile	96.49 ± 15.09	116.50 ± 23.84	-2.392	0.009
50th percentile	115.30 ± 12.63	142.05 ± 23.23	-4.645	<0.001
90th percentile	128.65 ± 13.01	161.30 ± 23.39	-5.610	<0.001
99th percentile	142.28 ± 18.89	183.5 ± 30.71	0.619	<0.001
VP				
Mean	126.92 ± 18.26	139.97 ± 18.61	-2.313	0.026
Variance	175.43 ± 171.57	206.65 ± 85.95	-1.044	0.307
Skewness	1.34 (-1.05,-0.16)	1.21 (-0.18,-0.64)	-0.860	0.390
Kurtosis	4.30 (1.23,5.63)	3.36 (0.73,4.09)	-0.842	0.400
1st percentile	80.84 ± 24.88	85.50 ± 26.93	-0.600	0.552
10th percentile	109.61 ± 21.09	116.30 ± 24.83	-0.965	0.341
50th percentile	128.30 ± 21.59	138.84 ± 21.97	-1.780	0.083
90th percentile	145.19 ± 28.75	153.70 ± 20.78	-1.377	0.316
99th percentile	157.86 ± 23.03	163.80 ± 18.51	-0.966	0.340

BCA, basal cell adenoma; PA, pleomorphic adenoma.

Table 3
Diagnostic efficiency of distinguishing PA and BCA by histogram parameters.

Parameters	AUC (95%CI)	Cutoff value	Sensitivity (%)	Specificity (%)
1st percentile of NC	0.722 (0.569,0.875)	63.00	81.00	64.40
mean of AP	0.863 (0.756,0.969)	126.27	71.43	88.00
variance of AP	0.789 (0.660,0.917)	189.86	95.20	66.00
10th percentile of AP	0.750 (0.608,0.893)	102.50	71.40	73.00
50th percentile of AP	0.829 (0.707,0.950)	119.50	85.70	77.00
90th percentile of AP	0.876 (0.779,0.973)	132.00	90.50	84.00
99th percentile of AP	0.851 (0.741,0.962)	156.00	76.20	86.00
mean of VP	0.680 (0.520,0.840)	125.61	72.80	66.60

AUC, area under the curve; BCA, basal cell adenoma; PA, pleomorphic adenoma.

is 0.876, the sensitivity and specificity of distinguishing PA from BCA are 90.50% and 84.00%, respectively. To holistically evaluate the diagnostic advantage of AP, we constructed a combined model integrating six significant AP parameters (mean, variance and 10th/50th/90th/99th percentiles). The DeLong test was employed to compare the AUC between the combined AP model and the top-performing single parameters from non-AP phases. The combined AP model achieved a significantly higher AUC (0.962, 95% CI: 0.914–1.000) than the 1st percentile of NC (AUC = 0.722, 95% CI: 0.569–0.875, P=0.004) and the mean of VP (AUC = 0.680, 95% CI: 0.520–0.840, P<0.001). These results confirm that AP histogram parameters have stronger discriminative ability compared with non-arterial phase parameters. The detailed statistical output is shown in Table 4.

Table 4
DeLong test of AUC for combined AP model and non-AP phases.

Parameter/Model	AUC (95% CI)	P value (vs combined)
Combined AP Model	0.962 (0.914,1.000)	-
1st percentile of NC	0.722 (0.569,0.875)	P=0.004
mean of VP	0.680 (0.520,0.840)	P<0.001

AUC, area under the curve.

Discussion

Both PA and BCA are commonly seen in women, presenting as painless masses. The imaging features are typically single, circular or elliptical, with clear boundary and the potential for malignant transformation.[18,19] PA patients' mean age is about 10 years younger than that of BCA.[20,21] In our study, PA and BCA patients' mean age were 41.50 ± 15.25 years and 53.00 ± 9.38 years, which is consistent with the results of the previous studies. In the previous reports, the average diameter of BCA was generally smaller than that of PA.[22] This trend was also observed in our study, although the difference was not statistically significant, possibly due to the uneven sample sizes.

PA typically exhibits a uniform density, with the degree of enhancement during the arterial phase is slightly lower than that during the venous phase, demonstrating asymptotic enhancement. BCA enhancement is characterised by early and significant continuous enhancement, which can be attributed to the abundant presence of capillaries and

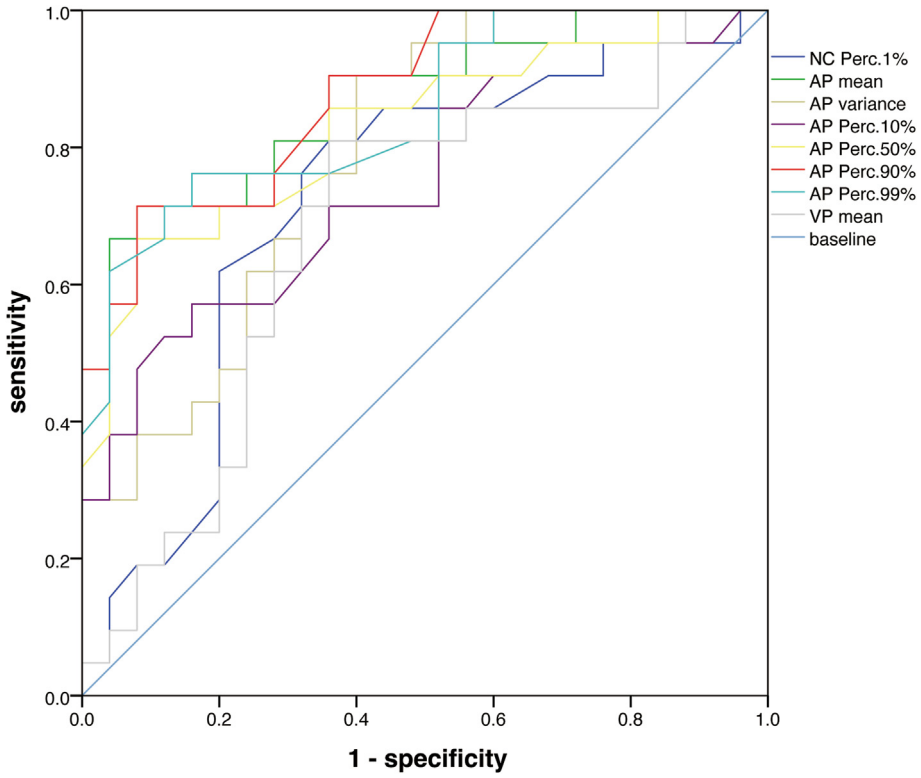

Figure 3 ROC curve analysis of histogram parameter in distinguishing PA and BCA. BCA, basal cell adenoma; PA, pleomorphic adenoma; ROC, receiver operating characteristic.

veins within the tumour. In this study, the enhancement values in the arterial and venous phases of PA were 47.31 ± 13.99 HU and 64.82 ± 18.26 HU, respectively. The enhancement values in the arterial and venous phases of BCA were 82.95 ± 23.34 HU and 95.10 ± 25.24 HU, respectively. The enhancement values for BCA were significantly higher than those for PA. In addition, we found that there were no statistical difference between PA and BCA groups in conventional imaging features such as location(superficial/deep), number(single/multiple), calcification(with/without), boundary(clear/unclear), shape(round/non-round) and cystic areas(with/without). This may be because these features can be found in both PA and BCA, and their specificity is low. Given the several overlapping features between BCA and PA, accurately distinguishing these tumours preoperatively is challenging. Therefore, it is crucial to accurately distinguish PA from BCA to guide individualised treatment plan and improve the prognosis of patients.

Texture analysis is a method that can quantitatively analyse the greyscale information of images. It uses objective indicators to characterise the microstructure and internal biological characteristics of the tumour tissue.[23,24] Histogram analysis is a useful texture analysis method, whose parameters can reflect the structure and heterogeneity of tumour tissue to a certain extent. For example, the mean can reflect the central trend and average level of data.[25] The degree of variance describes the dispersion of grey values. A higher degree of variance indicates greater deviation from the mean and stronger heterogeneity. This study conducted a detailed analysis of the histograms' parameters of NC, AP and VP for distinguishing PA and BCA. The results show that the AP mean of BCA is higher than that of PA, suggesting a higher overall brightness in BCA images. Furthermore, the AP variance of BCA is higher than that of PA, indicating greater brightness variation in BCA images. This finding further highlights the greater heterogeneity of BCA compared to PA. Pathologically, PA is composed of myoepithelial cells mixed with mucochondroid stroma, while BCA is classified into four different pathological subtypes: solid, tubular, trabecular and membranous, which further illustrates the diversity of BCA tumours. In addition, compared with NC and VP, AP histogram parameters are more beneficial in distinguishing parotid PA from BCA. The reason may be that PA is characterised by a mucinous cartilage like matrix and low vascular density, showing slow enhancement in the arterial phase and further enhancement in the venous phase; In contrast, BCA is composed of high vascular density basal-like cells, which exhibit significant enhancement in the early arterial phase. The differences in vascular characteristics and enhancement dynamics between the two are best identified during the arterial phase.[26]

The nth percentile represents the value below which a certain percentage of the research subjects fall.[27,28] The study reveals that numerical differences in percentiles are associated with tumour heterogeneity.[29] Specifically, there is a positive correlation between tumour heterogeneity and percentile values, where higher percentile values indicate greater heterogeneity among tumours. Our study found that when the 10th, 50th, 90th and 99th percentiles were used to differentiate PA and BCA, the AUC for evaluating the diagnostic efficiency of each parameter gradually increased with the percentile. Among them, the 90th percentile demonstrated the best grading diagnosis efficiency. This may be because higher percentiles can more accurately and objectively represent the internal structural characteristics of the tumour tissue, thus providing better diagnostic efficiency compared with lower percentiles. Similar to the findings of Xia *et al.*,[30] when CT-enhanced histogram parameters were used to distinguish pleomorphic adenoma from adenolymphoma, higher percentiles also showed the best differential diagnostic efficiency.

There are some limitations in this study: firstly, this study is a single-centre and retrospective study, and there may be some selective deviation due to the small sample size. Therefore, a larger multi-center study is needed to expand the sample size in the future. Secondly, this study only discusses histogram as the most commonly used first-order parameter in texture analysis, while higher-order parameters and advanced features have not been included. In order to further explore, the following research can use machine learning, deep learning and other algorithms for analysis.

Conclusions

In summary, CT-enhanced histogram analysis holds significant value in distinguishing between PA and BCA. The histogram parameters of the arterial phase exhibit greater advantages in differentiating PA from BCA, with the 90th percentile of the arterial phase demonstrating the highest diagnostic efficiency. This can serve as a reference for guiding individualised clinical treatment.

Funding

This study was supported by the Key R&D Program of Shaanxi Province, China (No. 2023-YBSF-673).

Author contribution

1. Guarantor of integrity of the entire study: X. Wu.
2. Study concepts and design; Manuscript editing: L. Han, X. Wu.
3. Literature research: M. Ma.
4. Clinical studies: H. Liu.
5. Experimental studies/data analysis: Q. Zhang, Y. Zhang, X. Liu.
6. Statistical analysis; Manuscript preparation: L. Han.

Conflict of interest

The authors declare no conflict of interest.

Acknowledgments

None.

Appendix A. Supplementary data

Supplementary data to this article can be found online at https://doi.org/10.1016/j.crad.2025.106934.

References

1. Gabelloni M, Faggioni L, Attanasio S, *et al*. Can magnetic resonance radiomics analysis discriminate parotid gland tumors? A pilot study. *Diagnostics (Basel)* 2020;**10**:900.
2. Almeslet AS. Pleomorphic adenoma: a systematic review. *Int J Clin Pediatr Dent* 2020;**13**:284–7.
3. Espinosa CA, Fernández-Valle A, Lequerica-Fernández R, *et al*. Clinicopathologic and surgical study of pleomorphic adenoma of the parotid gland: analysis of risk factors for recurrence and facial nerve dysfunction. *J Oral Maxillofac Surg* 2018;**76**:347–54.
4. Jeong AK, Lee HK, Kim SY, *et al*. Basal cell adenoma in the parapharyngeal space: MR findings. *Clin Imaging* 2001;**25**:392–5.
5. Cordeiro MS, de Freitas Filho SAJ, Servato JPS, *et al*. A retrospective study of 30 basal cell adenomas of the salivary gland in a Brazilian population and literature review. *Eur Arch Otorhinolaryngol* 2021;**278**:2447–54.
6. Chiu NC, Wu HM, Chou YH, *et al*. Basal cell adenoma versus pleomorphic adenoma of the parotid gland: CT findings. *AJR Am J Roentgenol* 2007;**189**:W254–61.
7. Yabuuchi H, Matsuo Y, Kamitani T, *et al*. Parotid gland tumors: can addition of diffusion-weighted MR imaging to dynamic contrast-enhanced MR imaging improve diagnostic accuracy in characterization? *Radiology* 2008;**249**:909–16.
8. Murayama Y, Kamitani T, Sagiyama K, *et al*. Evaluation of MR imaging findings differentiating parotid basal cell adenomas from other parotid tumors. *Eur J Radiol* 2021;**144**:109980.
9. Wallerius KP, Xie KZ, Lu LY, *et al*. Selective deep lobe parotidectomy vs total parotidectomy for patients with benign deep lobe parotid tumors. *JAMA Otolaryngol Head Neck Surg* 2023;**149**:1003–10.
10. Valstar MH, Mast H, Hove IT, *et al*. Malignant transformation of salivary gland pleomorphic adenoma: proof of principle. *J Pathol Clin Res* 2021;**7**:432–7.
11. Zoccali F, Cialente F, Colizza A, *et al*. Clinico-histopathological review of 255 patients who underwent parotidectomy for pleomorphic adenoma: a 10-year retrospective study-a proposal for an optimal diagnostic and therapeutic algorithm for patients with recurrent pleomorphic adenoma. *Eur Arch Otorhinolaryngol* 2023;**280**:3329–35.
12. Lubner MG, Smith AD, Sandrasegaran K, *et al*. CT texture analysis: definitions, applications, Biologic correlates, and challenges. *Radiographics* 2017;**37**:1483–503.
13. Ganeshan B, Miles KA. Quantifying tumour heterogeneity with CT. *Cancer Imaging* 2013;**13**:140–9.
14. Liu X, Pan YC, Zhang X, *et al*. A deep learning model for classification of parotid neoplasms based on multimodal magnetic resonance image sequences. *Laryngoscope* 2023;**133**:327–35.
15. Azoulay A, Cros J, Vullierme M-P, *et al*. Morphological imaging and CT histogram analysis to differentiate pancreatic neuroendocrine tumor grade 3 from neuroendocrine carcinoma. *Diagn Interv Imaging* 2020;**101**:821–30. 103353.
16. Xue CQ, Zhou Q, Zhang P, *et al*. MRI histogram analysis of tumor-infiltrating CD8+ T cell levels in patients with glioblastoma. *Neuroimage Clin* 2023;**37**:103353.
17. Skálová A, Hyrcza MD, Leivo I. Update from the 5th edition of the World Health organization classification of head and neck tumors: salivary glands. *Head Neck Pathol* 2022;**16**:40–53.
18. Hellquist H, Paiva-Correia A, Poorten VV, *et al*. Analysis of the clinical relevance of histological classification of benign epithelial salivary gland tumours. *Adv Ther* 2019;**36**:1950–74.
19. Kim H, Kim SY, Kim YJ, *et al*. Correlation between computed tomography imaging and histopathology in pleomorphic adenoma of parotid gland. *Auris Nasus Larynx* 2018;**45**:783–90.
20. Zhan KY, Khaja SF, Flack AB, *et al*. Benisubgn parotid tumors. *Otolaryngol Clin North Am* 2016;**49**:327–42.
21. Xu ZF, Yong F, Yu T, *et al*. Different histological subtypes of parotid gland tumors: CT findings and diagnostic strategy. *World J Radiol* 2013;**5**:313–20.
22. Zheng YL, Zheng YN, Li CF, *et al*. Comparison of different machine models based on multi-phase computed tomography radiomic analysis to differentiate parotid basal cell adenoma from pleomorphic adenoma. *Front Oncol* 2022;**12**:889833.
23. Vernuccio F, Arnone F, Cannella R, *et al*. Diagnostic performance of qualitative and radiomics approach to parotid gland tumors: which is the added benefit of texture analysis? *Br J Radiol* 2021;**94**:20210340.
24. Chen FF, Ge YQ, Li S, *et al*. Enhanced CT-based texture analysis and radiomics score for differentiation of pleomorphic adenoma, basal cell adenoma, and Warthin tumor of the parotid gland. *Dentomaxillofac Radiol* 2023;**52**:20220009.
25. Szczypinski PM, Strzelecki M, Materka A, *et al*. MaZda–a software package for image texture analysis. *Comput Methods Programs Biomed* 2009;**94**:66–76.
26. Yu Y, Zhang WB, Soh HY, *et al*. Efficacy of computed tomography features in the differentiation of basal cell adenoma and Warthin tumor in the parotid gland. *Oral Surg Oral Med Oral Pathol Oral Radiol* 2021;**132**:589–96.
27. Yang X, Knopp MV. Quantifying tumor vascular heterogeneity with dynamic contrast-enhanced magnetic resonance imaging: a review. *J Biomed Biotechnol* 2011;**2011**:732848.
28. Kerut EK, Given M, Giles TD. Review of methods for texture analysis of myocardium from echocardiographic images: a means of tissue characterization. *Echocardiography* 2003;**20**:727–36.
29. Nam SJ, Yoo J, Lee HS, *et al*. Quantitative evaluation for differentiating malignant and benign thyroid nodules using Histogram Analysis of Grayscale Sonograms. *J Ultrasound Med* 2016;**35**:775–82.
30. Xia FF, Guo FP, Liu Z, *et al*. Enhanced CT combined with texture analysis for differential diagnosis of pleomorphic adenoma and adenolymphoma. *BMC Med Imaging* 2023;**23**:169.